TOWARDS EFFECTIVE LARGE-SCALE REAL-TIME CONTROL SCHEME: STRUCTURAL IDENTIFICATION OF A HIGH-REYNOLDS NUMBER TURBULENT BOUNDARY LAYER VIA WALL SENSORS

[1]RASIYE BEIGZADEH, [2]M. B. ABBASSI, [3]M. R. ABBASSI

[1]Dept. Automotive Eng., Iran University of Science and Technology, Narmak, Tehran, Iran
[2]Dept. Mech. Eng., Sirjan University of Technology, Sirjan, Kerman Province, Iran
[3]Dept. Mech. Eng., The University of Melbourne, Parkville, VIC 3010, Australia
E-mail:[1]r_beigzadeh@auto.iust.ac.ir, [2]m.abbassi@sirjantech.ac.ir, [3]mrbe@student.unimelb.edu.au

Abstract - The large-scale coherent structures in the outer region of a high-Reynolds-number turbulent boundary layer are highly energetic and have an influence on the wall and hence on the skin friction drag. To evaluate the accuracy of the structural manipulation for large-scale real-time control schemes, in which wall sensors are utilized as control components, the canonical effect of the outer-region structures onto the wall needs to be quantified. We conducted measurements of friction velocity fluctuations (u_τ), together with simultaneous measurements of streamwise velocity (u) fluctuations throughout a turbulent boundary layer with a friction Reynolds number of $Re_\tau \approx 14400$. The streamwise locations for both of the measurements of the u and u_τ fluctuations were nominally the same. The coherence magnitude between the former and latter signals is evaluated as a function of the wall-normal height and the resolved streamwise wavelength. It is concluded that the most influential large-scale structures in the log-region of a high-Reynolds-number turbulent boundary layer on the wall-shear stress possess a characteristic lower bound of a streamwise wavelength of $\lambda_x \approx 1.9\delta$ (where δ is the boundary layer thickness).

Index Terms - Turbulent boundary layer, Coherent structures, High-Reynolds-number, Large-scale control scheme.

I. INTRODUCTION

Turbulent boundary layers (TBLs) comprise two major regions in the wall-normal direction: The near-wall region $0 \leq z^+ \leq 30$ and the outer region $0.02 \leq z/\delta \leq 1$, both of which are populated by coherent structures[1], [2], [3], and [4]. The wall-normal height is denoted by z. The superscript '+' represents normalization by the viscous scaling. That is $z^+ = zU_\tau/\nu$, where ν is the kinematic viscosity and $U_\tau = (\tau_w/\rho)^{1/2}$ is the mean friction velocity of the turbulent boundary layer and δ is the boundary layer thickness. Experimental results by [1] and [5] showed that streamwise-aligned packets of hairpin vortices reside in the outer layer of a turbulent boundary layer. Due to the spanwise vorticity of the heads of the hairpin vortices, large regions (of the order of δ) of relative streamwise momentum deficit are generated underneath these packets. These regions of momentum deficit are flanked on the lateral sides by regions of streamwise momentum surplus. Both former and latter regions are referred to as large-scale motions (LSMs). LSMs tend to align in the streamwise direction and form very large-scale motions (VLSMs) or superstructures as postulated by [6]. LSMs and VLSMs have a top-down influence which extend down to the wall and are manifested in the large-scale components of both the energy of the near-wall structures [7], [8] and the energy of the wall-shear stress fluctuations as direct superimpositions [9]. The characteristic Reynolds number of a wall-bounded flow is the friction Reynolds number, formulated as $Re_\tau \equiv \delta^+ \equiv \delta/(\nu/U_\tau)$, and defined as the ratio between the outer and viscous length-scales. At high Reynolds numbers (i.e. $Re_\tau \geq 2000$) the fluctuating energy associated with the LSMs and VLSMs populating the log-region becomes comparable to that of the small-scale structures in the near-wall region [9], [10], and [11], hence they have a significant influence on the wall-shear stress. For the purposes of practical applications of real-time large-scale TBL flow control, it is vital to predict the passage of the large-scale coherent structures as accurately as possible from wall sensors. In other words, for an effective real-time control strategy, the uncertainty in the outer-region structure manipulation should be minimized. To that end, the objective of this experimental investigation is to evaluate the level of influence of the large-scale coherent structures in the outer region of a high-Reynolds-number turbulent boundary layer onto the wall. Recently, [12] presented the coherence magnitude between velocity fluctuations derived from a stationary hot-wire at $z^+ = 4.3$ and a traversing hot-wire throughout the boundary layer. Similar analysis was also conducted by[13], in which they only evaluated the coherence magnitude between a wall-shear stress sensor and a downstream hot-wire sensor at a single wall-normal height of 10 wall units and 300 wall units downstream of the detection sensor. In this study, a hot-film sensor was utilized to measure the friction velocity (i.e. u_τ) fluctuations, together with a traversing hot-wire sensor for boundary layer measurements (i.e. u) located at the same streamwise and spanwise locations as that of the hot-film. As such, the nominal wall-normal location of the stationary sensor is $z^+ = 0$. Hot-wire anemometry methods were used to measure both the friction and streamwise velocity fluctuations. Throughout this article, x, y and z denote the streamwise, spanwise and wall-normal

directions of the flow, respectively. Hence, the corresponding fluctuating velocity components are, represented by u, v and w. The power spectral density and the wavenumber of the streamwise fluctuating velocity are denoted by ϕ_{uu} and k_x, respectively.

II. EXPERIMENTAL SET-UP

A. Flow Conditions

The experiments were conducted in the High Reynolds Number Boundary Layer Wind Tunnel (HRNBLWT) at the University of Melbourne. The flow conditions provided a boundary layer thickness of $\delta = 0.368\text{m}$ at the measurement section of the tunnel, which was chosen to be at $x = 21$ m downstream of the nozzle exit. This resulted in a friction velocity of $U_\tau = 0.641\text{ms}^{-1}$, together with a friction Reynolds-number of $Re_\tau = \frac{U_\tau \delta}{\nu} \approx 14400$.

B. Measuring Sensors

The hot-wire is made of a $d = 2.5\mu$m-diameter platinum wire mounted on a Dantec boundary layer probe (55P15) with offset prongs. The wire has an exposed sensing element of $l_{hw} = 0.5\text{mm}$, which provided a length-to-diameter ratio of $l_{hw}/d = 200$ (recommended by [14]). The hot-wire was operated with the Melbourne University Constant Temperature Anemometer (MUCTA) of in-house design with a sampling rate of $\Delta t^+ \approx 1.32$. The boundary layer survey was performed within the physical range of $0.3 < z < 525mm$, with 40 logarithmically spaced wall-normal heights. Wall-shear stress measurements, simultaneously with the streamwise velocity measurements via the hot-wire sensor, was carried out with a hot-film sensor located nominally below the traversing hot-wire sensor (illustrated in Fig. 1). The overheat ratios of the hot-wire and hot-film sensors were set to 1.72 and 1.50, respectively. The choice of the relatively low overheat ratio for the hot-film sensor is believed to minimize the mutual influence of these two sensors during the course of the boundary layer measurement, especially for those data points during which the hot-wire was in the proximity of the hot-film. The hot-film sensor was sampled at a sampling rate of $\Delta t^+ \approx 6.62$. The characteristics of these sensors are summarized in Table I.

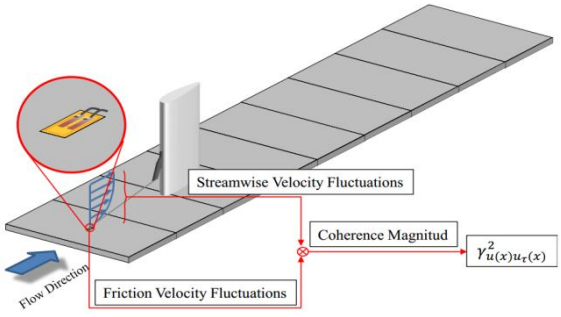


Fig. 1 Schematic of the set-up for simultaneous measurements of the friction velocity fluctuations ($u_\tau(x)$) and streamwise velocity fluctuations($u(x)$) throughout the turbulent boundary layer above the u_τ-measurements.

Table I: Sensor specifications.

Hot-wire sensor				Hot-film sensor		
l^+_{hw}	l_{hw}/d	$1/\Delta t$ (Hz)	Δt^+	l^+_{hf}	$1/\Delta t$ (Hz)	Δt^+
20	200	20 000	1.32	36	4 000	6.62

C. Calibration

The traversing probe was calibrated in situ against the streamwise velocity measured with a Pitot-static tube located in free-stream at 525mm above the wall. The calibration procedure for the hot-wire comprised pre- and post-calibration exercises. Each calibration exercise consisted of 16 measuring points ranging from a free-stream velocity of 0ms^{-1} to 24ms^{-1}. A fifth order polynomial curve is best fitted through each set of calibration data points, in a least-squares sense. Linear interpolation in time between the pre- and post-calibration curves is implemented to compensate for any probable temperature drift of the hot-wire sensor during the measurements. The hot-film sensor was calibrated in situ against the unit Reynolds number (i.e. U_∞ / ν). Using previously acquired wall-shear stress data via a floating element sensor [15], U_∞/ν could be converted to a unit friction Reynolds number U_τ/ν, and thus a friction velocity U_τ. However, since the hot-films were attached to a modular panel insert (made of Aluminum), heat of the sensors could conduct to the underlying surface. Consequently, temperature variations in the laboratory directly influence the output voltages of the sensors. In an effort to account for such **inevitable** data contamination, the calibration technique by [16]was adopted. This technique requires regular intervals of single point recalibration measurements, apart from the standard pre- and post-calibration processes. As such, the changes of the temperature of the substrate is empirically taken into account. Finite-order polynomial curves are fitted through the calibration data points in a least square sense—here a fifth order polynomial is used. As suggested by [16] a correction coefficient $(R|_i = (E_i - E_{pre})|_{U_\tau} / (E_{post} - E_{pre})|_{U_\tau})$ is calculated from the recalibration data point together with the pre- and post-calibration curves and a modified calibration curve is generated as follows:

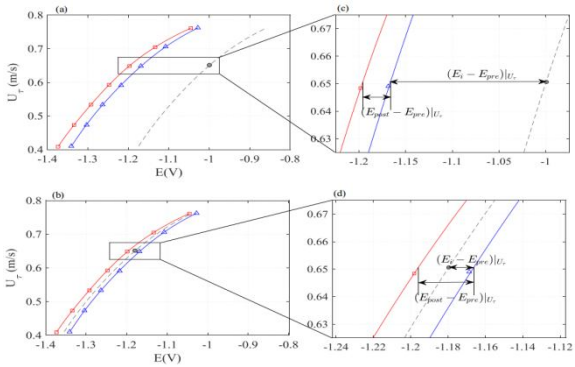


Fig. 2 The pre-calibration (Δ) and post-calibration (□) data points of the hot-film voltage against the friction velocity with their respective fifth order polynomial curve fits. Depending on the relative position of the single point (○) of the ith recalibration exercise, the corrected calibration curve (dashed line) is either extrapolated (a) or interpolated (b). (c) and (d) magnified views; illustrating how each term of the correction ratio ($R|_i = (E_i - E_{pre})|_{U_\tau} / (E_{post} - E_{pre})|_{U_\tau}$) is calculated.

$$E_{int}|_{U_\tau} = R|_i(E_{post}|_{U_\tau} - _E_{pre}|_{U_\tau}) + E_{pre}|_{U_\tau}. \quad (1)$$

Fig. 2(a–d) illustrates how the numerator and denominator of the correction coefficient is determined. Depending on the relative position of the recalibration data point with respect to the pre- and post-calibration ranges two different possibilities might occur:

1. the single point recalibration falls outside the pre- and post-calibration ranges. As such, extrapolation is implemented to calculate $R|_i$—Fig. 2(a), and
2. the single point recalibration falls between the pre- and post-calibration ranges. As such, interpolation is implemented to calculate $R|_i$—Fig. 2(b).

Since the hot-film sensors are only capable of resolving the large-scale fluctuations accurately, prior to converting the hot-film voltage fluctuations into the friction velocity fluctuations, they are convoluted in time with a 1.5δ Gaussian filter.

III. RESULTS AND DISCUSSION

A. Coherence Magnitude between u_τ and u

The coherence magnitude between the u_τ fluctuations and the simultaneous u fluctuations throughout the turbulent boundary layer above the u_τ measurements are evaluated in order to obtain the accuracy of large-scale manipulation. This coherence magnitude is presented in terms of the linear coherence spectrum, denoted as $\gamma^2_{uu_\tau}$, and formulated as:

$$\gamma^2_{uu_\tau} = \frac{|\phi_{uu_\tau}|^2}{\phi_{uu}\phi_{u_\tau u_\tau}}, \qquad 0 < \gamma^2_{uu_\tau} < 1 \quad (2)$$

where, ϕ_{uu_τ} is the complex-valued cross-spectrum, and ϕ_{uu} and $\phi_{u_\tau u_\tau}$ are the power spectra densities of the streamwise and friction velocity fluctuations, respectively. By physical description, the coherence magnitude between any two signals is a coefficient—bounded by 0 and 1—which indicates the level of correlation between the constituent respective spectral components of the two composing signals. For instance, if the γ^2-value of two signals is 1 at a certain wavelength, it implies that the amplitude of oscillation per unit standard deviation of these two signals at that particular wavelength are identical with each other. Here, the two signals are the streamwise velocity fluctuations (i.e. u) at each wall-normal height throughout the turbulent boundary layer and the simultaneous friction velocity fluctuations (i.e. u_τ). More details with regard to the coherence magnitude can be found in[12].

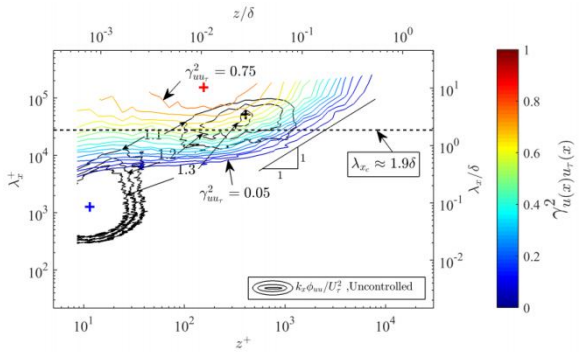


Fig. 3Iso-contours (colored contour lines) of the coherence magnitude for the streamwise velocity fluctuations relative to the large-scale friction velocity fluctuations at the same streamwise location as that of the velocity measurements. Contour levels vary from 0.05 to 0.75 with increments of 0.05. The peak of the coherence magnitude is shown by a red cross (+). Underlying are three contour levels, namely 1.1, 1.2 and 1.3 (black contour lines), of the pre-multiplied energy spectrum of the streamwise velocity fluctuations in a canonical flow. The corresponding inner- and outer-peaks of the spectrogram are demarcated by blue (+) and black (+) crosses, respectively.

The iso-contours of the calculated coherence magnitude are plotted in Fig. 3 as a function of the wall-normal height and the streamwise wavelength (colored contour lines).Additionally, three levels, namely 1.1, 1.2 and 1.3, of the pre-multiplied energy spectrogram (i.e. $k_x\phi_{uu}/u_\tau^2$) of the canonical turbulent boundary layer—black contour lines—are also plotted in Fig. 3. The iso-contours of $\gamma^2_{uu_\tau}$ possess a distinct peak—demarcated with a red cross (+) at the proximity of the outer peak of the energy spectrogram—demarcated with a black cross (+).

The lack of overlap of these two outer-peaks might indicate that the most energetic structures in the log-region of the TBL—under the investigated flow conditions ($Re_\tau \approx 14400$)—are not those ones that have the most influence on the wall. Akin to the pre-multiplied energy spectrogram of u fluctuations (is not shown here), the contour plots of the coherence magnitude of u and u_τ fluctuations is also predicted to possess an inner-peak in the proximity of the inner-peak of the spectrogram—demarcated as a blue cross (+) in Fig. 3. In other words, the influence of the energetic near-wall region structures on the wall should also be manifested in the coherence magnitude of the u and u_τ fluctuations. It might be deduced that since the hot-film sensors are not capable of resolving the high frequency fluctuations accurately, the inner-peak of the coherence magnitude is nullified.

It was also observed by [12] that the iso-contours of the coherence magnitude generated from their data does not possess any inner-peak either. They attributed this to the fact that the measurement data acquired via hot-wire anemometry is temporal data. Taylor's hypothesis together with the local mean streamwise velocity at each wall-normal height were used to convert temporal information to spatial information.

Since the small-scale coherent structures in the near-wall region have a large spread of convection velocities the usage of a single convection velocity in the Taylor's hypothesis at each wall-normal height distorts the spatial realization of the boundary layer in the near-wall region. Therefore, the coherence of the small-scale structures within that region appears to be annihilated. Because of the proximity of their stationary sensor to the wall (i.e. $z^+ = 4.3$) it can be predicted that any two-input/one-output analysis from [12] would exhibit strong resemblance with those presented here, where a glued-on hot-film sensor on the wall was utilized as the stationary sensor—given that the temporal resolution of the hot-film is similar to that of the hot-wire.

CONCLUSION

In this study, the coherence magnitude between large-scale component of the friction velocity fluctuations with the streamwise velocity fluctuations throughout a canonical turbulent boundary layer ($\gamma^2_{\hat{u}u_\tau}$) with a friction Reynolds number of $Re_\tau \approx 14400$ is quantified. It is shown that the large-scale structures with wave-lengths of 1.9δ and beyond have a significant influence onto the wall, inferred from the contour levels of $\gamma^2_{\hat{u}u_\tau}$. Therefore, it can be advised to the control community, who intend to conduct large-scale control strategies on turbulent boundary layers with practical Reynolds numbers, to have their control components tailored towards manipulating the coherent structures with characteristic length scales of the order of approximately 2δ and above. Since the measurements of the u fluctuations were carried out above the u_τ fluctuations, the analysis conducted in Section III can be regarded as an assessment of the accuracy of large-scale manipulations for a hypothetical real-time flow control scheme with zero time delay between the structural detection and actuation. However, in realistic selective control schemes, there is a finite latency between the former and the latter. This leads to a finite streamwise distance between the sensors and the actuators, which further compromises the accuracy of the manipulation. As such, further experimental campaign is under progress in order to investigate the coherence magnitude between u_τ fluctuations and simultaneous **downstream** u fluctuations throughout the turbulent boundary layer.

REFERENCES

[1] R. J. Adrian, C. D. Meinhart, and C. D. Tomkins, "Vortex organization in the outer region of the turbulent boundary layer," J. Fluid Mech., vol. 422, pp. 1–54, 2000.

[2] S. J. Kline, W. C. Reynolds, F. A. Schraubt, and P. W. Runstadlers, "The structure of turbulent boundary layers," J . Fluid Meeh, vol. 30, no. 4, pp. 741–773, 1967.

[3] J. Smits and I. Marusic, "Wall-bounded turbulence," Phys. Today, vol. 66, no. 9, pp. 25–30, 2013.

[4] Wark and H. M. Nagib, "Relation between outer structures and wall-layer events in boundary layers with and without manipulation." Illinios Institute of Technology, 1990.

[5] C. D. Tomkins and R. . J. Adrian, "Spanwise structure and scale growth in turbulent boundary layers," J. Fluid Mech., vol. 490, no. September 2003, pp. 37–74, 2003.

[6] K. C. Kim and R. J. Adrian, "Very large-scale motion in the outer layer," Phys. Fluids, vol. 11, no. 2, p. 417, 1999.

[7] J. JIMÉNEZ, J. C. DEL ÁLAMO, and O. FLORES, "The large-scale dynamics of near-wall turbulence," Journal of Fluid Mechanics, vol. 505. pp. 179–199, 2004.

[8] Marusic, R. Mathis, and N. Hutchins, "High Reynolds number effects in wall turbulence," Int. J. Heat Fluid Flow, vol. 31, no. 3, pp. 418–428, 2010.

[9] H. Abe, H. Kawamura, and H. Choi, "Very Large-Scale Structures and Their Effects on the Wall Shear-Stress Fluctuations in a Turbulent Channel Flow up to Re_tau=640," J. Fluids Eng., vol. 126, no. 5, p. 835, 2004.

[10] N. Hutchins and I. Marusic, "Large-scale influences in near-wall turbulence," Philos. Trans. R. Soc. A Math. Phys. Eng. Sci., vol. 365, no. 1852, pp. 647–664, 2007.

[11] Marusic, R. Mathis, and N. Hutchins, "Predictive model for wall-bounded turbulent flow.," Science, vol. 329, no. 5988, pp. 193–196, 2010.

[12] W. J. Baars, N. Hutchins, and I. Marusic, "Self-similarity of wall-attached turbulence in boundary layers," J. Fluid Mech., vol. 823, p. R2, 2017.

[13] R. Rathnasingham and K. S. Breuer, "System identification and control of a turbulent boundary layer," Phys. Fluids, vol. 9, no. 7, pp. 1867–1869, 1997.

[14] P. M. Ligrani and P. Bradshaw, "Spatial resolution and measurement of turbulence in the viscous sublayer using subminiature hot-wire probes," Exp. Fluids, vol. 5, no. 6, pp. 407–417, 1987.

[15] W. J. Baars, D. T. Squire, K. M. Talluru, M. R. Abbassi, N. Hutchins, I. Marusic, D. T. S. K. M, R. Abbassi, K. M. Talluru, N. Hutchins, and I. Marusic, "Wall-drag measurements of smooth- and rough-wall turbulent boundary layers using a floating element," Exp. Fluids, vol. 57, no. 5, pp. 1–16, 2016.

[16] M. Talluru, V. Kulandaivelu, N. Hutchins, and I. Marusic, "A calibration technique to correct sensor drift issues in hot-wire anemometry," Meas. Sci. Technol., vol. 25, no. 10, p. 105304:1-6, 2014.

★★★